ALZHEIMER'S DISEASE

Scanning ultrasound removes amyloid-β and restores memory in an Alzheimer's disease mouse model

Gerhard Leinenga and Jürgen Götz*

Amyloid-β (Aβ) peptide has been implicated in the pathogenesis of Alzheimer's disease (AD). We present a non-pharmacological approach for removing Aβ and restoring memory function in a mouse model of AD in which Aβ is deposited in the brain. We used repeated scanning ultrasound (SUS) treatments of the mouse brain to remove Aβ, without the need for any additional therapeutic agent such as anti-Aβ antibody. Spinning disk confocal microscopy and high-resolution three-dimensional reconstruction revealed extensive internalization of Aβ into the lysosomes of activated microglia in mouse brains subjected to SUS, with no concomitant increase observed in the number of microglia. Plaque burden was reduced in SUS-treated AD mice compared to sham-treated animals, and cleared plaques were observed in 75% of SUS-treated mice. Treated AD mice also displayed improved performance on three memory tasks: the Y-maze, the novel object recognition test, and the active place avoidance task. Our findings suggest that repeated SUS is useful for removing Aβ in the mouse brain without causing overt damage, and should be explored further as a noninvasive method with therapeutic potential in AD.

INTRODUCTION

Alzheimer's disease (AD) is characterized by the presence of soluble oligomers of amyloid-β (Aβ) peptide that aggregate into extracellular fibrillar deposits known as amyloid plaques (*1*–*3*). Aβ is elevated in the AD brain because of the increased production of this peptide and its impaired removal (*4*, *5*). Recent therapeutic strategies have targeted both processes (*6*), including the inhibition of secretase enzymes to reduce Aβ production, as well as active and, in particular, passive immunization approaches for boosting Aβ clearance. These strategies, however, have side effects. Inhibition of secretases affects additional substrates with potential off-target effects (*7*), and passive immunization may be costly once effectiveness is demonstrated in clinical trials (*8*).

Here, we aim to establish whether a transient opening of the blood-brain barrier (BBB) using repeated scanning ultrasound (SUS) could assist in Aβ clearance. Only one method has been demonstrated to open the BBB noninvasively and repeatedly, that is, nonthermal focused ultrasound coupled with intravenous injection of microbubbles, which are used as ultrasound contrast agents (*9*). Ultrasound delivery is based on the principle that biologically inert and preformed microbubbles comprising either a lipid or polymer shell, a stabilized gas core, and a diameter of less than 10 μm are systemically administered and subsequently exposed to noninvasively delivered focused ultrasound pulses (*10*). Microbubbles within the target volume become "acoustically activated" by what is known as acoustic cavitation. In this process, the microbubbles expand and contract with acoustic pressure rarefaction and compression over several cycles (*10*). This activity has been associated with a range of effects, including the displacement of the vessel wall through dilation and contraction (*11*, *12*). More specifically, the mechanical interaction between ultrasound, microbubbles, and the vasculature transiently opens tight junctions and facilitates transport across the BBB (*13*). In assessing ultrasound-induced BBB opening, previous studies reported no difference in BBB opening or closing between Aβ plaque–forming APP/PS1 mice and nontransgenic (non-Tg) littermate controls (*14*).

Clem Jones Centre for Ageing Dementia Research, Queensland Brain Institute, The University of Queensland, St Lucia Campus, Brisbane, Queensland 4072, Australia.
*Corresponding author. E-mail: j.goetz@uq.edu.au

Focused ultrasound allows for a transient opening of the BBB in the absence of tissue damage, as demonstrated in many experimental species, including rhesus macaques (*13*). In these primates, repeated opening of the BBB in the region of the visual cortex using focused ultrasound did not impair the ability of the animals to perform a complex visual acuity task in which they had been trained. Devices that emit ultrasound capable of penetrating the human brain are currently in clinical trials. Recently, a proof-of-concept study of using magnetic resonance–guided focused ultrasound to treat tremor and chronic pain has been successfully completed (*15*). Here, we investigate the use of SUS to remove Aβ from the AD mouse brain and to improve cognition and memory.

RESULTS

Scanning ultrasound is a safe method to transiently open the BBB

We first established in C57BL/6 non-Tg wild-type mice that the BBB can be opened repeatedly by ultrasound, either by using single entry points (as is conventionally done) or by using SUS across the entire brain (Fig. 1, A to C). Mice were anesthetized, injected intravenously with microbubbles together with the indicator dye Evans blue, and then placed under the focus of a TIPS (therapy imaging probe system) ultrasound transducer (Philips Research) (*16*). Subsequent brain dissection revealed that a single ultrasound pulse resulted in a 1-mm-wide blue column of Evans blue dye, demonstrating focused opening of the BBB (Fig. 1B). When the focus of the ultrasound beam was moved in 1.5-mm increments until the entire forebrain of the mouse was sonicated with SUS, the BBB was opened throughout the brain, as evidenced by prevalent extravasation of Evans blue dye as early as 30 min after the treatment (fig. S1, A and B). This was also illustrated by fluorescence imaging 30 min to 1 hour after treatment (Fig. 1C). We optimized the ultrasound settings and established that a 0.7-MPa peak rarefactional pressure, 10-Hz pulse repetition frequency, 10% duty cycle, and 6-s sonication time per spot were optimal. These settings did not cause "dark" neurons, reflecting degeneration, as revealed by Nissl staining (fig. S1, C and D), or edema or erythrocyte extravasation as shown by hematoxylin and eosin (H&E) staining (fig. S1, E to H). To determine whether SUS caused immediate damage, we analyzed non-Tg

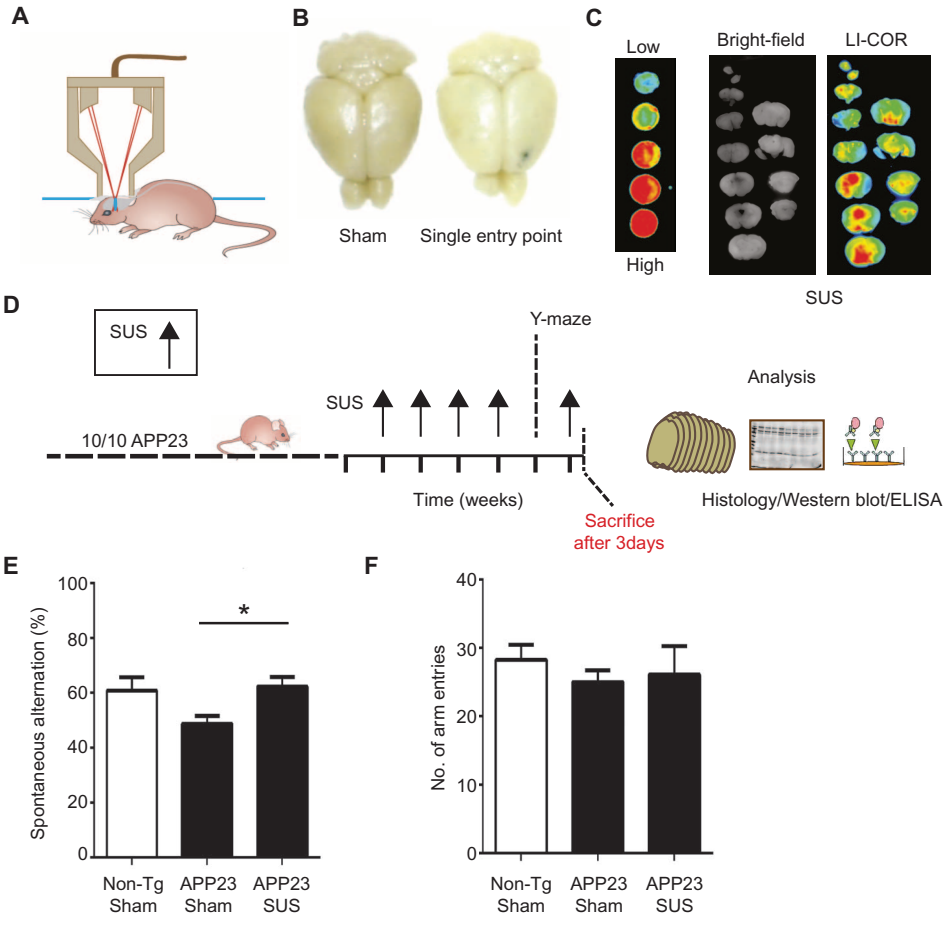

Fig. 1. Establishing SUS in an AD mouse model. (**A**) Setup of SUS equipment. (**B** and **C**) BBB opening by ultrasound was monitored by injecting wild-type mice with Evans blue dye that binds to albumin, a protein that is normally excluded from the brain. (B) A single entry point revealed a focal opening of the BBB in response to ultrasound treatment, with Evans blue dye able to enter the brain at this point. (C) Widespread opening of the BBB 1 hour after SUS was demonstrated with an Odyssey fluorescence LI-COR scanner of brain slices using nitrocellulose dotted with increasing concentrations of blue dye as a control. (**D**) Treatment scheme for the first cohort of hemizygous male Aβ plaque–forming APP23 mice (median age, 12.8 months). The mice received SUS or sham treatment for a total duration of the experiment of 6 weeks. Mice were randomly assigned to treatment groups. Using histological methods, Western blotting, enzyme-linked immunosorbent assay (ELISA), and confocal microscopy, we measured the effect of SUS treatment on amyloid pathology in mouse brain. Before the last SUS treatment, all mice were tested in the Y-maze. (**E**) The sequence of arm entries in the Y-maze was used to obtain a measure of alternation, reflecting spatial working memory. The percentage of alternation was calculated by the number of complete alternation sequences (that is, ABC, BCA, and CAB) divided by the number of alternation opportunities. Spontaneous alternation was restored in SUS-treated compared to sham-treated APP23 mice using non-Tg littermates as controls ($n = 10$ per group; one-way ANOVA followed by Dunnett's posttest, $P < 0.05$). (**F**) Total number of arm entries did not differ between groups.

mouse brain tissue 4 hours and 1 day after SUS treatment using acid fuchsin stain and found no evidence of ischemic damage (fig. S1, I and J).

SUS reduces Aβ and amyloid plaque load in plaque-forming APP23 transgenic mice

Having confirmed the viability of our protocol, we treated an initial cohort of 10 male Aβ plaque–forming APP23 transgenic mice five times with SUS over a period of 6 weeks (Fig. 1D, study design). At the age of 12 to 13 months, APP23 mice have a substantial plaque burden and spatial memory deficits (*17*). Age-matched APP23 mice in the control group ($n = 10$) received microbubble injections and were placed under the ultrasound transducer, but no ultrasound was emitted. After the 4-week sham or SUS treatment period, the mice underwent behavioral testing for a 2-week period in which they were not treated. We analyzed spatial working memory functions in the Y-maze. This test is based on the preference of mice to alternate between the arms of the maze. The analysis revealed that spontaneous alternation (calculated by the number of complete alternation sequences divided by the number of alternation opportunities) in APP23 mice treated with SUS, but not in sham-treated animals, was restored to wild-type levels [$P < 0.05$, one-way analysis of variance (ANOVA) followed by Dunnett's multiple comparison] (Fig. 1E). Total entries into the Y-maze arms did not differ between groups (Fig. 1F). The mice received one additional ultrasound treatment and were sacrificed 3 days later for histological and biochemical analysis.

We next used Campbell-Switzer silver staining to distinguish the compact core of mature amyloid plaques from more dispersed Aβ deposits (Fig. 2, A and B). By analyzing every eighth section from −0.8 to −2.8 mm from bregma for each mouse (total of 8 to 10 sections per mouse), we found that the cortical area occupied by plaques was reduced by 56% ($P = 0.014$, unpaired t test) (Fig. 2C) and that the average number of plaques per section was reduced by 52% ($P = 0.017$, unpaired t test) (Fig. 2D) in SUS-treated compared to sham-treated mice. Thioflavin-S staining (Fig. 2E) and immunohistochemistry with the Aβ-specific antibody 4G8 (Fig. 2F) were used to confirm the specificity of the silver staining. We also plotted plaque load, as determined in Fig. 2C, as a function of age and included untreated mice to demonstrate the baseline of plaque load at the onset of treatment (Fig. 2G). It remains to be determined how our protocol would need to be modified to reveal efficacy in inducible models of AD, such as tetO-APPswe/ind mice (*18*).

We then extracted the right hemisphere from 10 SUS-treated and 10 sham-treated APP23 mice and used these tissues to obtain two lysates, one fraction enriched in extracellular proteins and a Triton-soluble fraction (*19*). By Western blotting with antibodies against Aβ, we were able to identify different species of the peptide (Fig. 3, A and B). The concentrations of these Aβ species were quantified, and reductions were found in the extracellular fraction for SUS-treated compared to sham-treated mice for high molecular weight species (HMW; 58% reduction), *56 oligomeric Aβ (Aβ*56; 38% reduction) and the trimeric Aβ/toxic APP C-terminal fragment (3-mer/CTFβ; 29% reduction) (Fig. 3C),

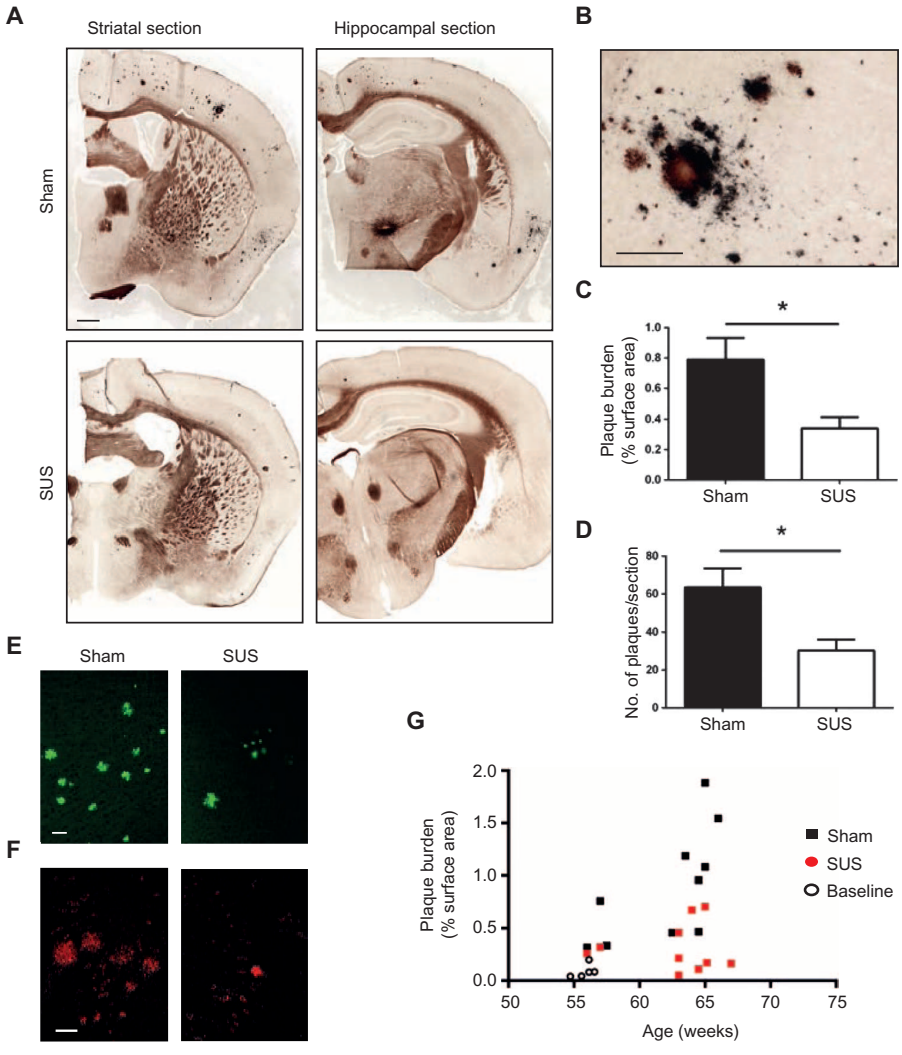

Fig. 2. SUS reduces Aβ plaques in an AD mouse model. (**A** and **B**) Representative images of free-floating coronal sections from APP23 transgenic mice (first cohort) with and without SUS treatment. Campbell-Switzer silver staining revealed compact, mature plaques (amber) and more diffuse Aβ deposits (black). A stained section at a higher magnification is shown in panel (B). (**C** and **D**) Quantification of amyloid plaques revealed a 56% reduction in the area of cortex occupied by plaques (unpaired *t* test, $P = 0.017$) and a 52% reduction in plaque number per section (*t* test, $P = 0.014$) in SUS-treated compared to sham-treated APP23 mice ($n = 10$ per group). (**E** and **F**) Representative sections of SUS-treated brains versus control brains stained with Thioflavin S (E) and 4G8 (F). (**G**) Plaque load plotted as a function of age confirmed that the SUS-treated group had significantly lower plaque load than the sham-treated group. Baseline plaque load at the onset of treatment is indicated by open circles. Scale bars, 1 mm (panel A) and 200 μm (panel B).

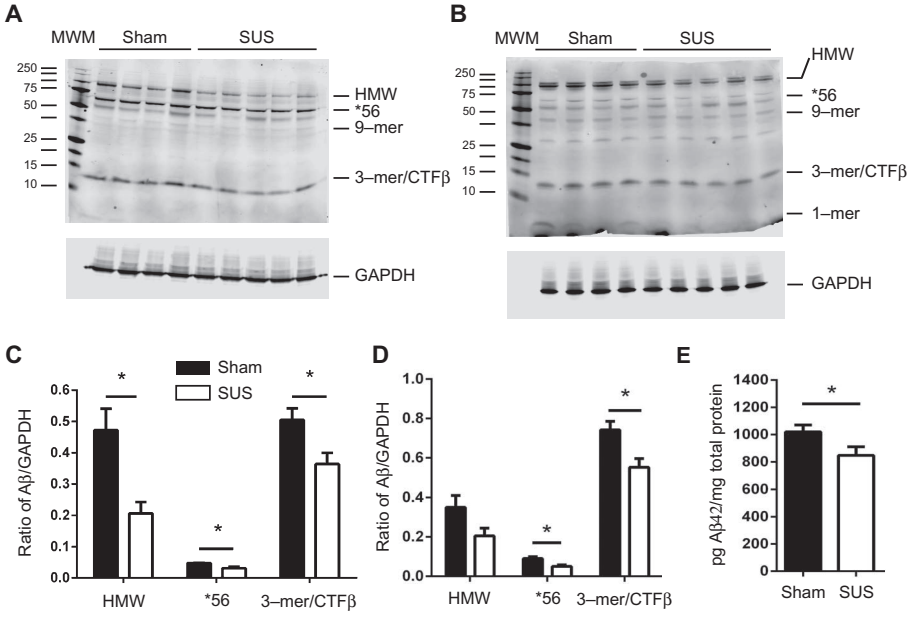

Fig. 3. SUS treatment reduces different Aβ species. (**A** to **D**) Western blotting of extracellular-enriched (A) and Triton-soluble (B) fractions of the brains of the first cohort of APP23 mice with 6E10 and 4G8 anti-Aβ antibodies revealed a reduction in distinct Aβ species in both fractions in SUS-treated compared to sham-treated mice. These data are quantified in (C) and (D), respectively. The Western blots show significant reductions of HMW species, the 56-kD oligomeric Aβ*56 (*56) and trimeric Aβ (3-mer)/CTFβ, in the extracellular-enriched fraction and of *56 and 3-mer/CTFβ in the Triton-soluble fraction (unpaired *t* tests, $P < 0.05$). GAPDH (glyceraldehyde 3-phosphate dehydrogenase) was used for normalization. MWM, molecular weight marker. (**E**) ELISA for Aβ42 in the Triton-soluble fraction revealed a significant reduction in SUS-treated compared to sham-treated mouse brains (unpaired *t* test, $P < 0.05$; $n = 10$ per group).

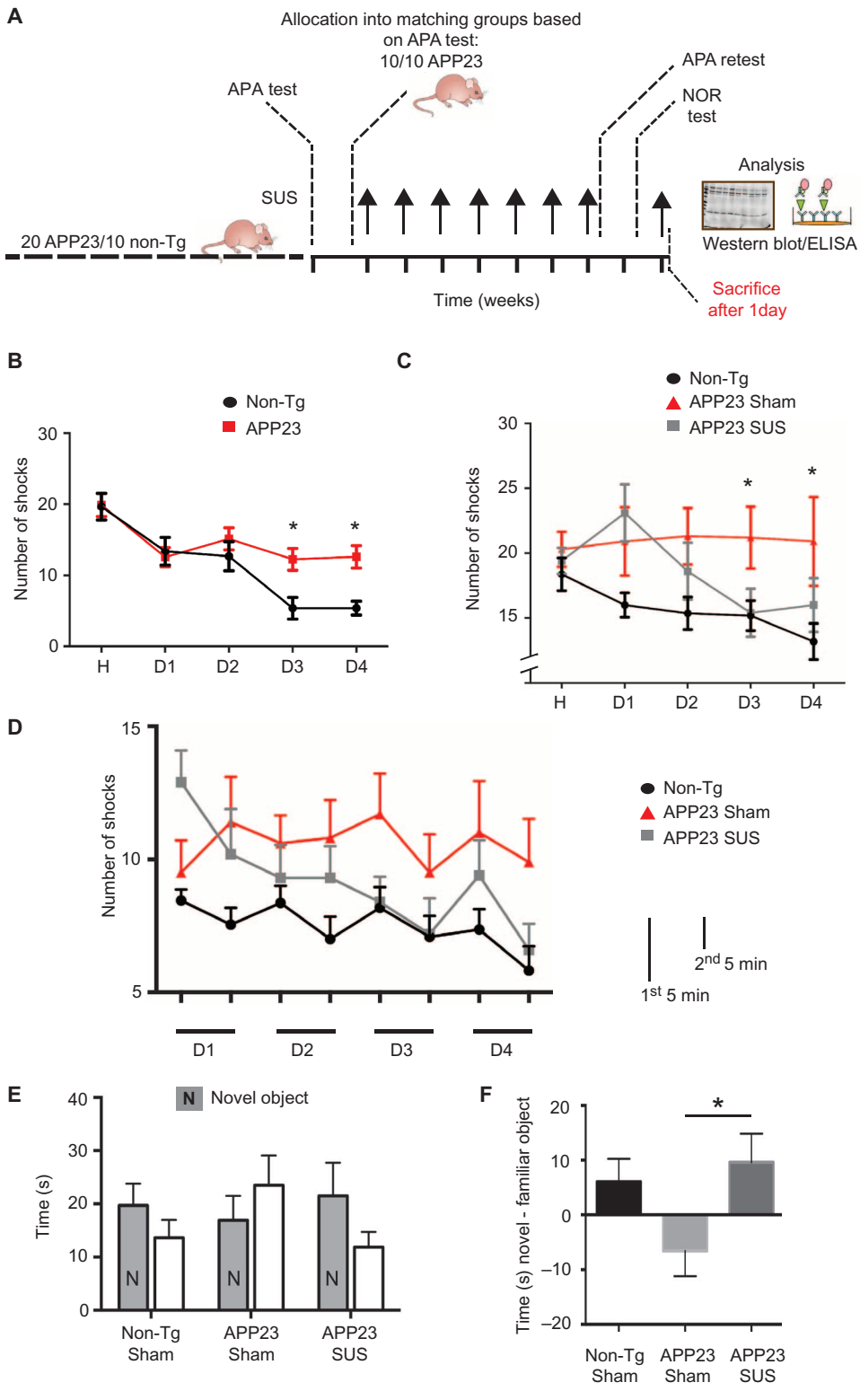

Fig. 4. SUS treatment rescues memory deficits in an AD mouse model. (**A**) Treatment scheme of a second cohort of 20 gender-matched APP23 mice and 10 non-Tg littermates to determine the functional outcome of the SUS treatment protocol in more robust behavioral tests. The mice were analyzed in the APA task, a test of hippocampus-dependent spatial learning in which mice learned to avoid a shock zone in a rotating arena. After the APA test, the APP23 mice were divided into two groups with matching performance and received weekly SUS or sham treatment for 7 weeks. This was followed by an APA retest and a novel object recognition (NOR) test. One day after the final SUS treatment, mice were sacrificed and brain extracts were analyzed by Western blotting and ELISA. (**B**) Twenty APP23 mice and 10 non-Tg littermates tested in the APA test, with a habituation session (labeled H) followed by four training sessions (labeled D1 to D4). (**C**) In the APA retest, SUS-treated mice showed better learning than did sham-treated mice when tested for reversal learning ($P = 0.031$). (**D**) SUS-treated mice also showed improvement when the first 5 min (long-term memory) and last 5 min (short-term memory) were plotted separately ($P = 0.031$). (**E**) The APA retest was followed by the NOR test to determine the time spent with the novel object (labeled N) compared with the familiar object. (**F**) Analysis of the discrimination ratio that divides the above measure by the total time spent exploring both objects revealed that SUS-treated APP23 mice showed an increased preference for the novel object compared to sham-treated APP23 mice ($P = 0.036$).

and in the Triton-soluble fraction for *56 (50%) and trimeric Aβ/CTFβ (27%) ($P < 0.05$, unpaired t tests) (Fig. 3D). ELISA revealed a 17% reduction for $A\beta_{42}$ in the Triton-soluble fraction of SUS-treated compared to sham-treated mice (unpaired t test, $P < 0.05$; $n = 10$ per group) (Fig. 3E).

SUS treatment restores memory functions in AD mice

To determine the functional outcome of our SUS treatment protocol in more robust behavioral tests, we next analyzed a second cohort of 20 gender-matched APP23 mice and non-Tg littermates ($n = 10$) in the active place avoidance (APA) task, a test of hippocampus-dependent spatial learning in which mice learn to avoid a shock zone in a rotating arena (Fig. 4A, study design). APP23 mice and non-Tg littermates underwent 4 days of training after habituation. There were significant effects of day of training ($F_{3,84} = 5.49$, $P = 0.002$) and genotype ($F_{1,28} = 5.41$, $P = 0.028$, two-way ANOVA), with day as the within-subjects factor (Fig. 4B). APP23 mice were divided into two groups with matching performance on the APA test and received weekly SUS or sham treatment for 7 weeks. Mice were retested in the APA test with the location of the shock zone

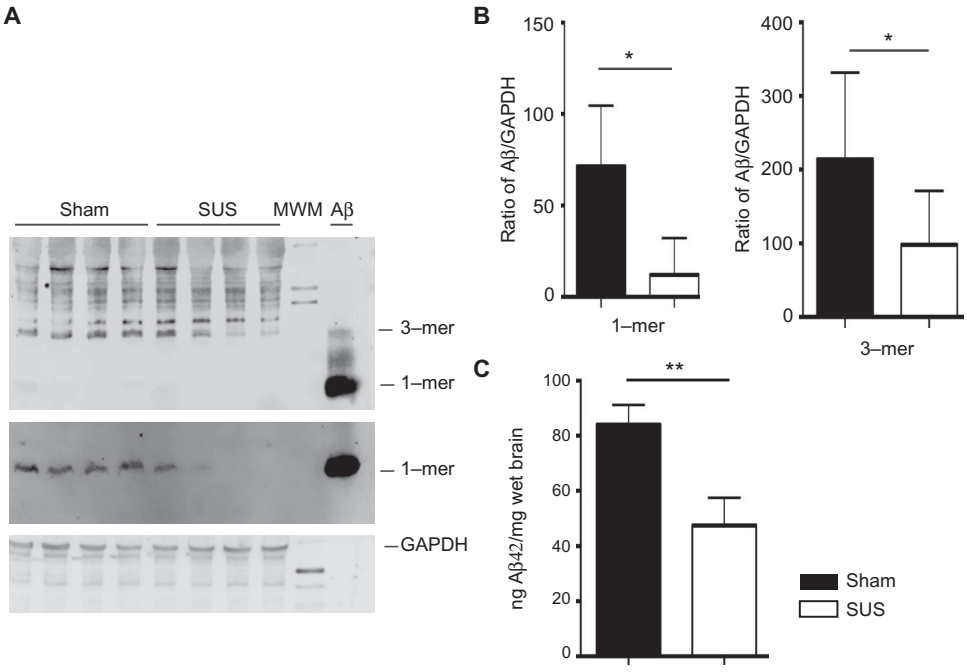

Fig. 5. SUS treatment reduces Aβ in a second cohort of AD mice. (**A**) A second cohort of APP23 mice was analyzed by Western blot with the anti-Aβ antibody W0-2; gel and transfer conditions were optimized to reveal the monomer and trimer specifically. The monomer was efficiently captured by using two sandwiched membranes. (**B**) The blots showed significant reduction of the monomer (fivefold reduction) and trimer (twofold reduction) in the extracellular fraction (unpaired *t* tests, $P < 0.05$). (**C**) ELISA for Aβ42 in the guanidine-insoluble fraction revealed a twofold reduction in SUS-treated compared to sham-treated mice (unpaired *t* test, $P < 0.008$; $n = 10$ per group).

in the opposite area of the arena (reversal learning). In the retest, there was a significant effect of day ($F_{3,84} = 2.809$, $P = 0.044$) and treatment group ($F_{2,28} = 3.933$, $P = 0.0312$). Multiple comparisons test for simple effects within rows showed that SUS-treated mice received fewer shocks on days 3 ($P = 0.012$) and 4 ($P = 0.033$) (Fig. 4C). SUS-treated mice also showed improvement when the first 5 min (long-term memory) and the last 5 min (short-term memory) of their performance were plotted separately ($F_{2,28} = 3.951$, $P = 0.0308$) (Fig. 4D). We also performed an NOR test, which revealed improved performance after SUS treatment, with SUS-treated mice showing a preference for the novel object (labeled N, Fig. 4, E and F) [$F_{2,28} = 2.99$, $P = 0.066$; $t(20) = 2.33$, $P = 0.0356$] compared to sham-treated control animals.

Upon sacrifice, we conducted a Western blot analysis using the Aβ-specific antibody W0-2, which showed a fivefold reduction of the monomer and a twofold reduction of the trimer in SUS-treated compared to sham-treated APP23 mice (unpaired *t* tests, $P < 0.05$) (Fig. 5, A and B). ELISA of the guanidine-insoluble brain fraction revealed a twofold reduction in $A\beta_{42}$ in SUS-treated samples ($P < 0.008$, unpaired *t* test) (Fig. 5C). Together, these data demonstrate that SUS has a robust effect on Aβ and memory function in AD mice.

SUS treatment causes uptake of Aβ into microglial lysosomes and clearance of plaques

Our results revealed that the degree of Aβ reduction achieved by SUS treatment was comparable to that achieved by passive Aβ immunization (*20*, *21*), but SUS treatment worked without the need for an additional therapeutic agent, such as antibodies, against Aβ. For passive vaccinations, different mechanisms have been proposed to remove Aβ from the brain (*22*, *23*), with variable effects on microglial activation (*20*, *24*). We therefore investigated whether microglial activation had an active mechanistic role in Aβ reduction caused by SUS treatment. On the basis of spinning disk confocal microscopy, an initial investigation of our first cohort of mice demonstrated that the microglia in SUS-treated brains fragmented and engulfed plaques (Fig. 6, A to D). We found that the microglia in SUS-treated APP23 mice contained twofold ($P = 0.002$, unpaired *t* test) more Aβ in lysosomal compartments than observed in sham-treated APP23 mice, as shown by costaining for Aβ and the microglial lysosomal marker CD68 (Fig. 6E). High-resolution three-dimensional (3D) reconstruction revealed extensive Aβ internalization in SUS-treated compared with sham-treated brains (Fig. 6, F to I, and movie S1). Confocal analysis of Aβ and CD68 further revealed cleared plaques in cortical areas in SUS-treated mice in which Aβ was almost completely contained in microglial lysosomes. This finding was observed in 75% of the SUS-treated mice but not in any of the sham-treated mice (Fisher's exact test, $P = 0.007$; $n = 8$ per group), with four sections analyzed in each case) (Fig. 6J).

SUS treatment induces microglial activation

We next sought to determine whether microglia in SUS-treated compared to sham-treated APP23 mice differed in other characteristics using sham-treated non-Tg littermates as control. Using the microglial cytoplasmic marker Iba1 (ionized calcium–binding adaptor molecule 1) (Fig. 7, A to C), we first determined the total microglial surface area, but we did not find differences between the three groups (*t* test) (Fig. 7D); there was also no difference in the size of microglial cell bodies (*t* test) (Fig. 7E). Resting microglia have highly branched extensions unlike activated phagocytic microglia. To quantify the extent of branching, after staining with the activated microglial marker Iba1, we converted the images to binary images that were then skeletonized (to obtain the most accurate tree geometry possible) (fig. S2, A to C). In this analysis, both the summed microglial process endpoints and the summed process length were normalized per cell using the Analyze Skeleton plugin in ImageJ (National Institutes of Health) (Fig. 7F). This showed that microglia in the SUS-treated group were more activated, a finding that was also reflected by a fivefold increase in the area of immunoreactivity for CD68 (*t* test, $P = 0.001$), a specific marker of microglial and macrophage lysosomes (Fig. 7, G to I).

Albumin may have a putative role in mediating Aβ uptake by microglia

Phagocytosis of Aβ by microglia and perivascular macrophages has been shown to be assisted by blood-borne immune molecules, including Aβ-specific antibodies (*20*). Another Aβ-neutralizing molecule is

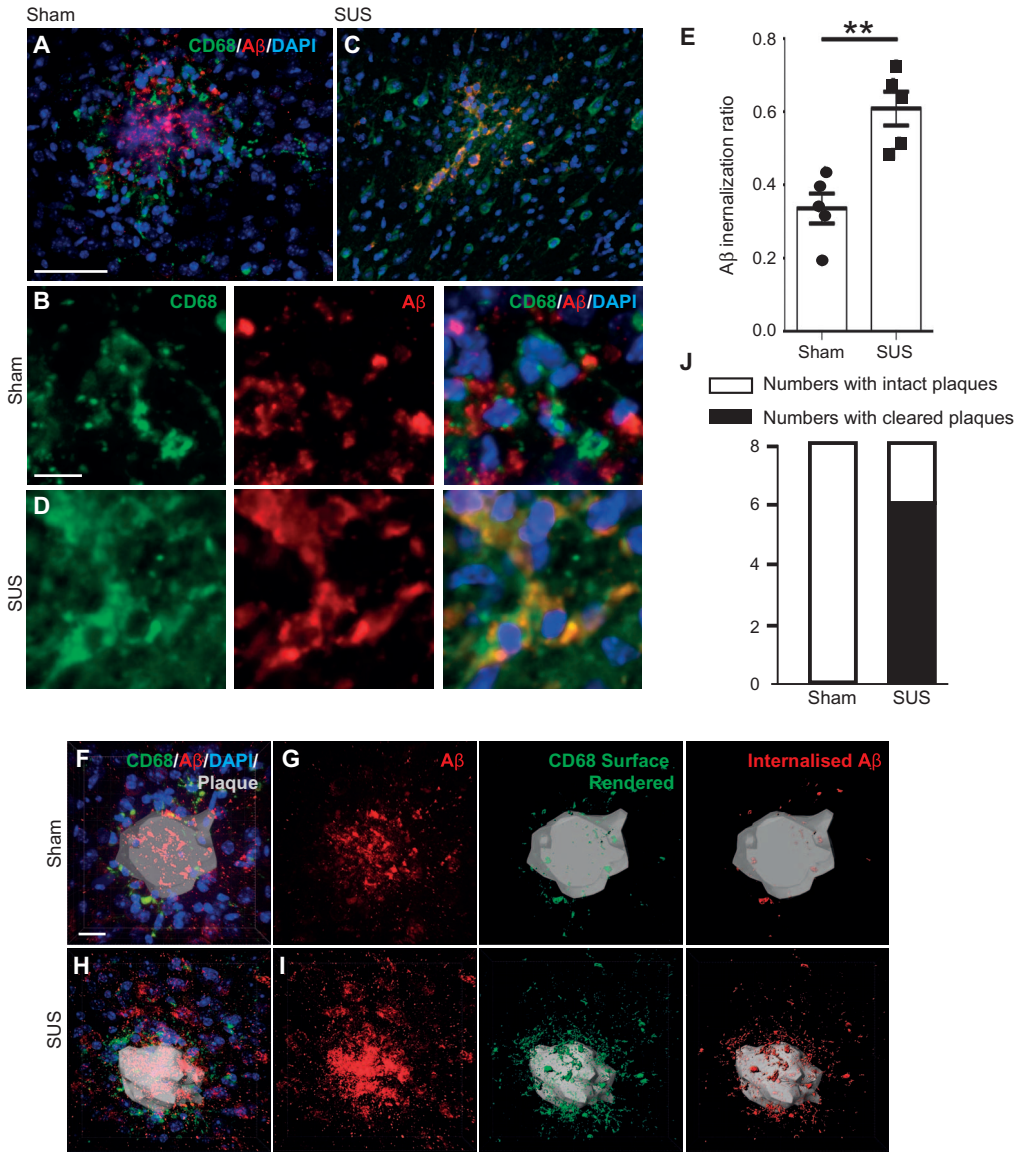

Fig. 6. Microglial phagocytosis and lysosomal uptake of Aβ induced by SUS treatment. (**A** and **B**) Plaques in sham-treated animals were surrounded by lysosomal CD68-positive microglia that contained some Aβ. (**C** and **D**) In contrast, plaques in SUS-treated mouse brains were surrounded by microglia that contained significantly more Aβ in their lysosomal compartments, with some plaques appearing to be completely phagocytosed by microglia. (**E**) A twofold increase in microglia-internalized Aβ was observed in SUS-treated compared to sham-treated mouse brains (unpaired *t* test, $P = 0.002$). (**F** to **I**) Plaques imaged at high magnification in 3D. CD68 labeling revealed the extent of Aβ at the plaque site that was internalized by microglia into lysosomes. 4′,6-Diamidino-2-phenylindole (DAPI) was used to visualize nuclei. (**J**) Confocal analysis of Aβ and CD68 revealed that 6 of 8 SUS-treated mice and 0 of 8 sham-treated mice had "cleared plaques" in cortical areas, with Aβ being almost completely within microglial lysosomes (Fisher's exact test, $P = 0.007$; $n = 8$ per group, with four sections analyzed in each case). Scale bars, 100 μm (A and C) and 10 μm (B, D, and F to I).

albumin, which is present in the blood and may establish a "peripheral sink" (*25*), although some reports argue against such a gradient (*26*). The fact that Evans blue dye–bound albumin can be detected in the brain after SUS treatment suggested to us that albumin may assist in Aβ engulfment not only in the periphery but also in the brain. After BBB disruption by ultrasound, albumin enters the brain where it is rapidly phagocytosed by glial cells but not by neurons (*27*). Albumin has also been demonstrated to bind to Aβ and inhibit its aggregation (*28*). To determine whether albumin may facilitate Aβ uptake by microglia, we incubated microglial BV-2 cells in culture with $A\beta_{42}$ with and without albumin (10 mg/ml; equivalent to 20% of the concentration in human serum) and found a 65% increase in $A\beta_{42}$ uptake in the presence of albumin (*t* test, $P = 0.0188$) (fig. S3). This result suggested that after SUS treatment, albumin may enter the brain and bind to Aβ, facilitating microglial phagocytosis. However, further work needs to be done to demonstrate a role for albumin in Aβ uptake by microglia in vivo.

Inflammation is not observed in SUS-treated mice

To determine whether additional microglia-independent mechanisms could be involved in Aβ clearance, we also investigated whether the Aβ-degrading enzyme IDE (insulin-degrading enzyme) was up-regulated by SUS. Western blot analysis revealed no significant difference between SUS-treated and sham-treated APP23 mice, although there was a trend toward an increase in IDE in SUS-treated mice (fig. S4, A and B). Because the microtubule-associated protein tau becomes phosphorylated in response to Aβ, we also performed Western blot using the phosphotau-specific antibody AT8, but phosphorylation was too variable to reveal a difference between groups (fig. S4, C and D).

Finally, we determined whether SUS up-regulated inflammatory markers associated with tissue damage. We first assessed the astrocytic marker GFAP (glial fibrillary acidic protein) and found an increased immunoreactivity (percentage of immunoreactive area) in APP23 compared to non-Tg mice, but no difference between SUS-treated and sham-treated APP23 mice (fig. S5, A and B). We also investigated the nuclear localization of the transcription factor NF-κB (nuclear factor κB), a marker of excessive, chronic inflammation. NF-κB–positive nuclei were absent in wild-type mice. In APP23 mice, they were confined to plaques, but we did not observe differences between SUS-treated and sham-treated animals (fig. S5, C and D). To complement the GFAP and Iba1 staining done in chronically treated APP23 mice (Fig. 7, A to F and fig. S5, A

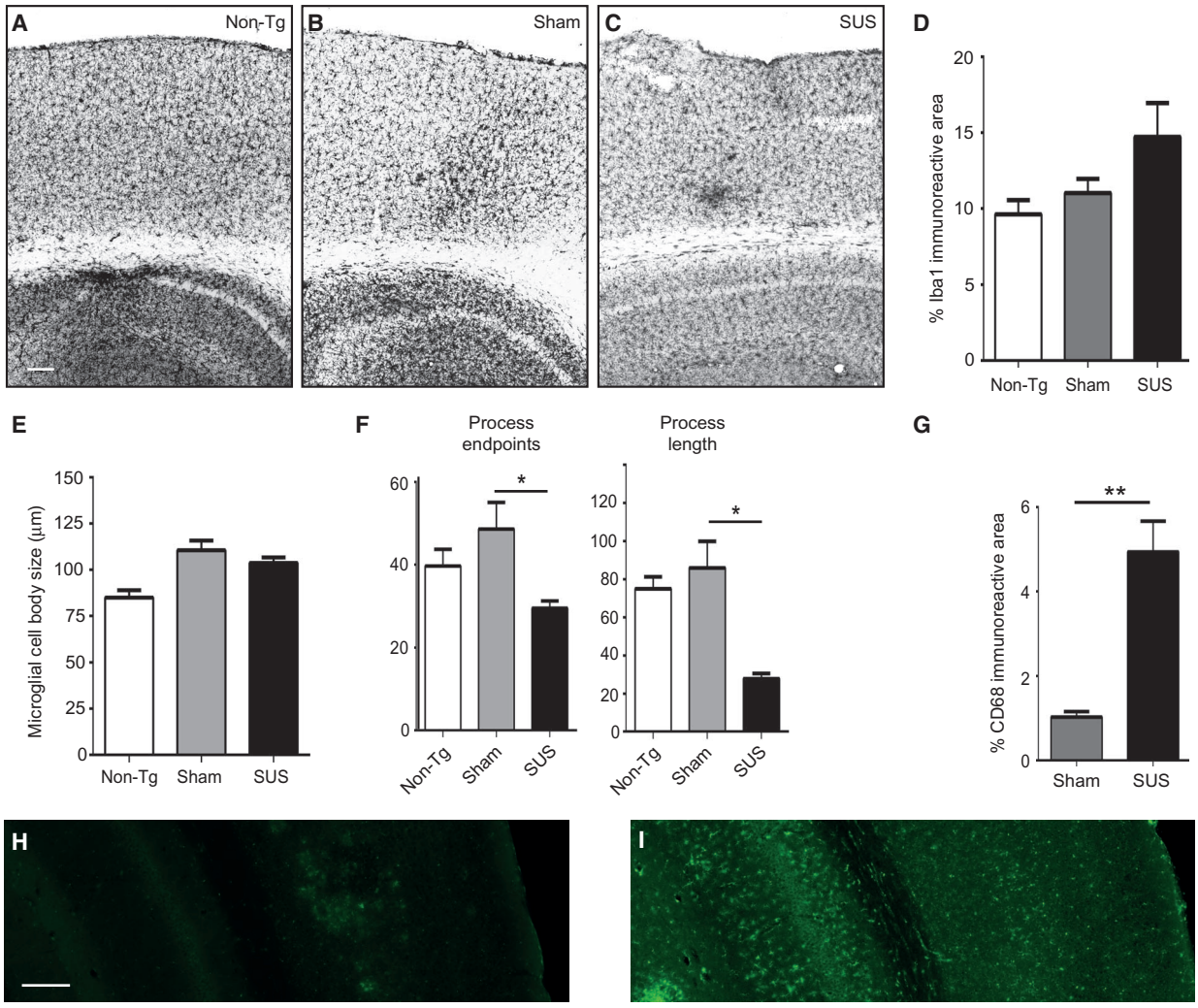

Fig. 7. Altered morphology after ultrasound but unaltered numbers of microglia in SUS-treated mice. (**A** to **C**) Sections of non-Tg mice (A) and sham-treated (B) and SUS-treated APP23 mice (C) stained with the microglial marker Iba1. (**D**) The microglial surface area did not differ between the three groups. (**E**) There was also no difference in the size of microglial cell bodies between the three groups. (**F**) A skeleton analysis in which both the summed microglial process endpoints and the summed process length were normalized per cell showing that microglia in the SUS-treated group were more activated (one-way ANOVA followed by Dunnett's posttest, $P < 0.05$) (D to F: $n = 4$, non-Tg; $n = 10$, sham-treated and SUS-treated). (**G** to **I**) This is also reflected by the fivefold increase in the surface area of CD68 immunoreactivity (G), a marker of microglial and macrophage lysosomes, in SUS-treated (I) compared with sham-treated (H) APP23 mice ($n = 10$, sham-treated and SUS-treated; t test, $P = 0.001$). Scale bars, 100 μm (A to C, H, and I).

and B), we also assessed GFAP and Iba1 reactivity in wild-type mice after acute treatment 1 and 24 hours after SUS. Iba1 staining revealed early activation of microglia at 1 and 24 hours, but astrogliosis was not detected using the GFAP-specific antibody (fig. S6, A to F). Together, our analysis suggested that SUS treatment did not lead to damaging inflammation.

DISCUSSION

Our results revealed that SUS treatment engages microglia and promotes internalization of Aβ into microglial lysosomes, thereby reducing Aβ and plaque load in the APP23 transgenic mouse model of AD as well as restoring function in tests of spatial and recognition memory. Although we have shown that SUS treatment induces microglia to effectively clear Aβ, it is equally possible that ultrasound and the transient opening of the BBB also attenuates the deposition of newly generated Aβ. This latter possibility has not been addressed in our study. It is, however, an important point if this technique were to be tried in humans at a stage where there was little plaque growth; the APP23 mice in our study were treated during a period of robust new amyloid deposition (Fig. 2G). Because Aβ-depositing animal models lack the full AD pathology, the effect of SUS on more comprehensive pathologies, including massive neuronal loss, also remains to be determined. Although it could be argued that, in a clinical setting, reductions in Aβ and plaque load may not inevitably lead to improved patient outcomes, our study clearly shows that a reduction in amyloid is associated with a restoration of performance in three independent memory-related behavioral tests.

At this stage, several hurdles have to be faced for SUS to be considered for application in human patients. In addition to the limitation presented by the animal model used in our study, it needs to be considered that the human brain is much larger than that of a mouse. Also, the thicker human skull presents an obstacle that needs to be factored in when parameters are defined that have the envisaged biological effect in the absence of tissue damage. There may also be the necessity to use one of several cranial windows to access the human brain. Also, if one were to apply SUS in humans at the prodromal stage before overt symptoms of AD were present, the safety of this approach would need to be monitored in real time. This could be facilitated by the recent development of advanced methods, such as passive cavitation detection, which is currently being evaluated in both rodents and primates (*29*). To avoid potentially excessive immune activation in a clinical setting (*30*), the ultrasound treatment regimen could possibly be done stepwise, covering one brain area at a time. Whereas we only coupled ultrasound with microbubbles, previous studies in rodents evaluated ultrasound for the delivery of therapeutic agents, such as antibodies (*31*, *32*), viral vectors (*33*), and dextran of different sizes (*9*, *10*). One study targeted Aβ using a few entry points for delivery and only a single treatment (*34*). Because the effect on Aβ plaques was very modest, the authors of this study suggested that focused ultrasound would best be suited as a delivery tool, for example, to boost the uptake of peripherally administered anti-Aβ antibodies (*34*). Our results, however, demonstrated that repeated SUS treatment of the entire mouse brain was sufficient to markedly ameliorate the pathology of Aβ-depositing mice as analyzed histologically, biochemically, and behaviorally. Our study highlights the potential of SUS treatment as a therapeutic approach for AD and possibly other diseases involving protein aggregation. However, this does not rule out the possibility that it could also be used as a vehicle for drug or gene delivery, given that the BBB remains the major obstacle for the uptake by brain tissue of therapeutic agents from the circulation (*9*).

MATERIALS AND METHODS

Study design

The study aimed to investigate how SUS treatment affects Aβ, plaque load, microglial phagocytosis of Aβ, and spatial memory. To this end, we treated and analyzed two cohorts of aged APP23 mice. A first cohort of hemizygous male APP23 mice (median age, 12.8 months) received SUS or sham treatment for the total duration of the experiment, which is 6 weeks (Fig. 1D). Mice were randomly assigned to treatment groups. Using histological methods, Western blotting, ELISA, and confocal microscopy, we measured the effect of SUS treatment on amyloid pathology in mouse brain.

A second cohort of gender-balanced APP23 mice was tested together with non-Tg mice in the APA memory test (Fig. 4A). After this initial testing, the APP23 mice were assigned to treatment groups on the basis of matching performance in the APA test (for details of the behavioral tests, see Supplementary Materials). The median age of the SUS-treated group was 67 weeks, and the median age of the sham-treated group was 65.6 weeks (range, 54 to 70 weeks for each group). After a 7-week period of treatment in which mice were given SUS or sham treatment, they were retested in the APA task. This was followed by the NOR behavioral test and then a final SUS or sham treatment. Using Western blotting and ELISA, we measured the effect of SUS treatment on amyloid pathology in this second cohort. The treatment condition was kept blinded until the analysis.

All animals were included in the analysis (except for the Western blots of the second cohort to determine monomer and trimer levels, where only eight mice were analyzed in each case). Sample sizes were chosen on the basis of previous experience and studies of this type conducted by others.

Animal models and ethics

APP23 mice express hAPP751 with the Swedish double mutation under the control of the murine Thy1.2 promoter (*35*). APP23 mice are characterized by pronounced mature amyloid plaques, mainly in the cortex, as well as associated memory deficits. Animal experimentation was approved by the Animal Ethics Committee of the University of Queensland (approval number QBI/027/12/NHMRC).

SUS equipment

An integrated focused ultrasound system was used (TIPS, Philips Research) (*16*). The system consisted of an annular array transducer with a natural focus of 80 mm, a radius of curvature of 80 mm, a spherical shell of 80 mm with a central opening 31 mm in diameter, a 3D positioning system, and a programmable motorized system to move the ultrasound focus in the x and y planes to cover the entire brain area. A coupler mounted to the transducer was filled with degassed water and placed on the head of the mouse with ultrasound gel for coupling, to ensure propagation of the ultrasound to the brain. The focal zone of the array was an ellipse of about 1.5 mm × 1.5 mm × 12 mm.

Antibodies and reagents

Antibodies to Aβ peptide epitope 1–16 (6E10) and 17–24 (4G8) were from Covance. Antibody to Aβ peptide epitope 4–10 (WO-2) was from Millipore. Antibodies to CD68 were from AbD Serotec (MCA195TT), to CD45 from AbD Serotec (MCA1031GA), to Iba1 or AIF1 (allograft inflammatory factor 1) from Millipore (MABN92), to GAPDH from Millipore (ABS16), to NF-κB p65 from Cell Signaling Technology (8242), and to human PHF-Tau (AT8) from Pierce Thermo Fisher (MN1020). Secondary antibodies were from Invitrogen, Cell Signaling Technology, LI-COR, and Dako. The Human Amyloid-β42 ELISA kit was from Millipore (EZH542). Total protein levels were assayed with a BCA (bicinchoninic acid) kit from Pierce (23227). Chemical reagents and human serum albumin were from Sigma-Aldrich.

Production of microbubbles

Lipid-shelled microbubbles with an octafluoropropane core were manufactured and characterized in-house. A 1:5:2:1 mass ratio of polyethylene glycol 6000, distearoyl-phosphatidylcholine, distearoylphosphatidylethanolamine, and pluronic F68 was dissolved in a 0.9% solution of NaCl. The solution was added to glass high-performance liquid chromatography vials, and air was removed and replaced with octafluoropropane gas to fill the headspace of the vial (Arcadophta). On the day of use, vials were heated to 37°C and were then shaken in a dental amalgamator for 40 s at 4000 rpm. The concentration and size of microbubbles were examined under a microscope and were found to be 1×10^7 to 5×10^7 microbubbles/ml with a size range of 1 to 10 μm and a mean diameter of 4 μm.

SUS application

Mice were anesthetized with Zoletil (20 mg/kg) and xylazine (10 mg/kg), and the hair on the head was shaved and depilated. Mice were injected

retro-orbitally with microbubble solution (1 μl/g) and then placed under the ultrasound transducer with the head immobilized (intravenous injections were also tested but proved less efficacious because of the small tail veins of mice). Parameters for the ultrasound delivery were 0.7-MPa peak rarefactional pressure, 10-Hz pulse repetition frequency, 10% duty cycle, 1 MHz center frequency, and 6-s sonication time per spot. The motorized positioning system moved the focus of the transducer array in a grid with 1.5 mm between individual sites of sonication so that ultrasound was delivered sequentially to the entire brain. For sham treatment, mice received all injections and were placed under the ultrasound transducer, but no ultrasound was emitted.

Monitoring BBB opening and damage to brain tissue

To determine successful opening of the BBB, 2% solution of Evans blue dye in 0.9% NaCl (4 ml/kg) was injected together with microbubbles (4 ml/kg), and SUS or sham treatment was performed as described above. Evans blue dye was >99% bound to albumin in the blood and the BBB was impermeable before treatment. After 30 min, mice were deeply anesthetized, transcardially perfused with phosphate-buffered saline (PBS) followed by 4% paraformaldehyde (PFA), and photographed under a stereo microscope (Carl Zeiss). To determine damage, sections from SUS-treated mice were stained with H&E to assess erythrocyte extravasation and tissue damage as well as with cresyl violet (Nissl staining) to assess neuronal damage. We further used the acid fuchsin stain (Santa Cruz Biotechnology) to detect ischemic neurons as described (*31*). Additional markers assessed were NF-κB and GFAP.

Tissue processing

Mice were deeply anesthetized with pentobarbitone before being perfused with 30 ml of ice-cold PBS. The brains were dissected from the skull and cut along the midline. The left hemisphere was fixed in 4% (w/v) PFA for 24 hours, cryoprotected in 30% sucrose, and sectioned coronally at 40-μm thickness on a freezing-sliding microtome. A one-in-eight series of sections was stored in PBS with sodium azide at 4°C until staining. The right hemisphere of the brain was frozen in dry ice or ethanol slurry and stored at −80°C until used for biochemical analysis.

Assessment of amyloid plaque load

A one-in-eight series of coronal brain sections were cut at 40-μm thickness on a microtome. An entire series of sections was processed for Campbell-Switzer silver staining (*36*) using a protocol available online at http://neuroscienceassociates.com/Documents/Publications/campbell-switzer_protocol.htm. For plaque counting, an entire one-in-eight series of sections was stained using the Campbell-Switzer method, and all sections −0.85 mm to −2.8 mm from bregma were analyzed (8 to 10 sections per mouse) after being photographed at ×16 magnification on a bright-field slide scanner. Plaque load in the cortex was obtained by the Particle Analysis plugin of ImageJ on coded images of sections using the area fraction method.

Skeleton analysis

A skeleton analysis to obtain the most accurate tree geometry possible was applied to quantify microglial morphology in images obtained from fixed brains as described (*37*). In brief, 40-μm sections were stained with Iba1 using the nickel-diaminobenzidine method. Two images from the auditory cortex overlying the dorsal hippocampus (an area rich in plaques) were each converted to binary images and then skeletonized using the Analyze Skeleton plugin by ImageJ. This plugin tags all pixel/voxels in a skeleton image and then counts all its junctions, triple points, and branches and measures their average and maximum length. The number of summed microglial process endpoints and summed process length normalized to the number of microglia were determined.

Spinning disk confocal microscopy and 3D rendering

Confocal imaging was conducted using a spinning disk confocal head (CSU-W1; Yokogawa Electric) coupled to a motorized inverted Zeiss Axio Observer Z1 microscope equipped with a 20/0.8 Plan-Apochromat air objective and a 100×/1.4 Plan-Apochromat oil objective (Carl Zeiss). Slidebook (version 5.5, Intelligent Imaging Innovations Inc.) was used to control the instrument and acquire optically sectioned images on an ORCA-Flash4.0 V2 sCMOS camera (Hamamatsu) with a pixel size of 6.5 μm × 6.5 μm (2048 × 2048 total pixels).

The imaging configuration described above achieves an XY pixel resolution of 0.31 μm and 0.1 μm for the 20× and 63× objectives, respectively. For analysis, image Z-stacks were acquired, with a Z-step size of 1.2 μm and 0.4 μm for the 20× and 63× objectives, respectively. Exposure times (100 to 800 ms) were maintained consistently for each marker across all experiments, and care was taken to avoid any incidence of pixel saturation.

Resulting 3D image data sets were analyzed using Imaris 7.4 (Bitplane). Microglia (CD68-positive) were identified using an automatic surface segmentation tool. These surfaces were subsequently used to mask Aβ labeling. The volume of this microglia-internalized portion of Aβ labeling was measured using the surface segmentation tool. 3D rendering of plaques was achieved using contouring and manual surface creation tools. For evaluation of the proportion of Aβ contained within microglial lysosomes, five sham-treated and five SUS-treated mice were analyzed, and differences were tested with a *t* test.

Protein extraction

We performed a serial extraction of brains to obtain fractions enriched for extracellular and Triton-soluble fraction proteins as described elsewhere (*19*). The forebrain of the right hemisphere was placed in 4× (w/v) of buffer containing 50 mM tris-HCl (pH 7.6), 0.01% NP-40, 150 mM NaCl, 2 mM EDTA, 0.1% SDS, 1 mM phenylmethanesulfonyl fluoride (PMSF), and complete protease inhibitors (Roche). The tissue was dissociated using a syringe and a 19-gauge needle, and the solution was centrifuged at 800*g* for 10 min to extract soluble extracellular proteins. Triton-soluble and intracellular proteins were obtained by homogenizing the intact cell pellet in 4 volumes of 50 mM tris-HCl, 150 mM NaCl, and 1% Triton X-100 and centrifuging for 90 min at 16,000*g*. To obtain the guanidine-insoluble fraction, the pellet was extracted in 5 M guanidine HCl followed by two centrifugations at 16,000*g* for 30 min each. Total protein concentration was determined by BCA assay (Pierce). All extraction steps took place at 4°C, and aliquots of the samples were stored at −80°C until use.

Western blotting

Forty micrograms each of extracellular-enriched and Triton-soluble proteins was separated on 10 to 20% tris-tricine gels (Bio-Rad) and were transferred onto 0.45-μm nitrocellulose membranes, using *N*-cyclohexyl-3-aminopropanesulfonic acid buffer (Bio-Rad) together with 20% methanol. A second membrane was used to capture the Aβ monomer. For antigen retrieval, the membranes were microwaved on a high setting for 30 s and stained briefly in Ponceau S to check transfer and equal loading. To visualize Aβ species, the membranes were then blocked in

PBS containing Odyssey blocking reagent (LI-COR) and incubated overnight in a 1:2000 dilution of 6E10 (for cohort 1; Covance) or a 1:2000 dilution of WO-2 (for cohort 2; Millipore). Rabbit anti-GAPDH antibody (1:2000; Millipore) was used as a loading control. Membranes were then blotted with anti-mouse immunoglobulin G (IgG)–IR680 and anti-rabbit IgG–IR800 fluorescent secondary antibodies (LI-COR) and were imaged on a LI-COR Odyssey scanner with detection setting of intensity 4.0 for the 700 channel and intensity 0.5 for the 800 channel. Signals from detected bands were quantified using Image Studio software (LI-COR). To determine AT8 and IDE levels, 10% tris gels were used, followed by transfer of the proteins onto 0.45-μm low-fluorescence polyvinylidene difluoride membranes.

Enzyme-linked immunosorbent assay

For detection of Aβ by ELISA, we quantified the levels of $Aβ_{1-42}$ in the Triton-soluble fraction (first cohort) and guanidine fraction (second cohort) using ELISA kits from Millipore (EZH542).

Statistics

Statistical analyses were conducted with Prism 6 software (GraphPad). Values were always reported as means ± SEM. One-way ANOVA with Dunnett's post hoc test was used for three groups, two-way ANOVA was used for APA, and unpaired *t* test was used to compare two groups. Where there was significant difference in variance between groups, we applied Welch's correction.

SUPPLEMENTARY MATERIALS

www.sciencetranslationalmedicine.org/cgi/content/full/7/278/278ra33/DC1
Methods
Fig. S1. Absence of brain damage after either repeated or short-term SUS treatment.
Fig. S2. Skeleton analysis of microglia.
Fig. S3. Increased Aβ uptake by microglial cells in the presence of albumin.
Fig. S4. Analysis of IDE and tau phosphorylation after SUS treatment in AD mice.
Fig. S5. Analysis of SUS-treated mice for inflammatory markers.
Fig. S6. Absence of astrogliosis but activation of microglia after acute ultrasound treatment in wild-type mice.
Movie S1 (mp4 format). High-resolution 3D reconstruction of a plaque imaged in a 40-μm section of a SUS-treated mouse.

REFERENCES AND NOTES

1. C. Haass, D. J. Selkoe, Soluble protein oligomers in neurodegeneration: Lessons from the Alzheimer's amyloid β-peptide. *Nat. Rev. Mol. Cell Biol.* **8**, 101–112 (2007).
2. M. Necula, R. Kayed, S. Milton, C. G. Glabe, Small molecule inhibitors of aggregation indicate that amyloid β oligomerization and fibrillization pathways are independent and distinct. *J. Biol. Chem.* **282**, 10311–10324 (2007).
3. L. M. Ittner, J. Götz, Amyloid-β and tau—A toxic pas de deux in Alzheimer's disease. *Nat. Rev. Neurosci.* **12**, 65 (2011).
4. D. Scheuner, C. Eckman, M. Jensen, X. Song, M. Citron, N. Suzuki, T. D. Bird, J. Hardy, M. Hutton, W. Kukull, E. Larson, E. Levy-Lahad, M. Viitanen, E. Peskind, P. Poorkaj, G. Schellenberg, R. Tanzi, W. Wasco, L. Lannfelt, D. Selkoe, S. Younkin, Secreted amyloid β-protein similar to that in the senile plaques of Alzheimer's disease is increased in vivo by the presenilin 1 and 2 and APP mutations linked to familial Alzheimer's disease. *Nat. Med.* **2**, 864–870 (1996).
5. K. G. Mawuenyega, W. Sigurdson, V. Ovod, L. Munsell, T. Kasten, J. C. Morris, K. E. Yarasheski, R. J. Bateman, Decreased clearance of CNS β-amyloid in Alzheimer's disease. *Science* **330**, 1774 (2010).
6. F. Mangialasche, A. Solomon, B. Winblad, P. Mecocci, M. Kivipelto, Alzheimer's disease: Clinical trials and drug development. *Lancet Neurol.* **9**, 702–716 (2010).
7. B. De Strooper, R. Vassar, T. Golde, The secretases: Enzymes with therapeutic potential in Alzheimer disease. *Nat. Rev. Neurol.* **6**, 99–107 (2010).
8. C. A. Lemere, E. Masliah, Can Alzheimer disease be prevented by amyloid-β immunotherapy? *Nat. Rev. Neurol.* **6**, 108–119 (2010).
9. E. E. Konofagou, Optimization of the ultrasound-induced blood-brain barrier opening. *Theranostics* **2**, 1223–1237 (2012).
10. J. J. Choi, K. Selert, F. Vlachos, A. Wong, E. E. Konofagou, Noninvasive and localized neuronal delivery using short ultrasonic pulses and microbubbles. *Proc. Natl. Acad. Sci. U.S.A.* **108**, 16539–16544 (2011).
11. S. B. Raymond, J. Skoch, K. Hynynen, B. J. Bacskai, Multiphoton imaging of ultrasound/Optison mediated cerebrovascular effects in vivo. *J. Cereb. Blood Flow Metab.* **27**, 393–403 (2007).
12. C. F. Caskey, S. M. Stieger, S. Qin, P. A. Dayton, K. W. Ferrara, Direct observations of ultrasound microbubble contrast agent interaction with the microvessel wall. *J. Acoust. Soc. Am.* **122**, 1191–1200 (2007).
13. N. McDannold, C. D. Arvanitis, N. Vykhodtseva, M. S. Livingstone, Temporary disruption of the blood-brain barrier by use of ultrasound and microbubbles: Safety and efficacy evaluation in rhesus macaques. *Cancer Res.* **72**, 3652–3663 (2012).
14. J. J. Choi, S. Wang, T. R. Brown, S. A. Small, K. E. Duff, E. E. Konofagou, Noninvasive and transient blood-brain barrier opening in the hippocampus of Alzheimer's double transgenic mice using focused ultrasound. *Ultrason. Imaging* **30**, 189–200 (2008).
15. N. Lipsman, M. L. Schwartz, Y. Huang, L. Lee, T. Sankar, M. Chapman, K. Hynynen, A. M. Lozano, MR-guided focused ultrasound thalamotomy for essential tremor: A proof-of-concept study. *Lancet Neurol.* **12**, 462–468 (2013).
16. R. Seip, C. T. Chin, C. S. Hall, B. I. Raju, A. Ghanem, K. Tiemann, Targeted ultrasound-mediated delivery of nanoparticles: On the development of a new HIFU-based therapy and imaging device. *IEEE Trans. Biomed. Eng.* **57**, 61–70 (2010).
17. L. M. Ittner, Y. D. Ke, F. Delerue, M. Bi, A. Gladbach, J. van Eersel, H. Wölfing, B. C. Chieng, M. J. Christie, I. A. Napier, A. Eckert, M. Staufenbiel, E. Hardeman, J. Götz, Dendritic function of tau mediates amyloid-β toxicity in Alzheimer's disease mouse models. *Cell* **142**, 387–397 (2010).
18. S. W. Fowler, A. C. Chiang, R. R. Savjani, M. E. Larson, M. A. Sherman, D. R. Schuler, J. R. Cirrito, S. E. Lesné, J. L. Jankowsky, Genetic modulation of soluble Aβ rescues cognitive and synaptic impairment in a mouse model of Alzheimer's disease. *J. Neurosci.* **34**, 7871–7885 (2014).
19. S. Lesné, M. T. Koh, L. Kotilinek, R. Kayed, C. G. Glabe, A. Yang, M. Gallagher, K. H. Ashe, A specific amyloid-β protein assembly in the brain impairs memory. *Nature* **440**, 352–357 (2006).
20. A. Wang, P. Das, R. C. Switzer 3rd, T. E. Golde, J. L. Jankowsky, Robust amyloid clearance in a mouse model of Alzheimer's disease provides novel insights into the mechanism of amyloid-β immunotherapy. *J. Neurosci.* **31**, 4124–4136 (2011).
21. J. L. Frost, B. Liu, M. Kleinschmidt, S. Schilling, H. U. Demuth, C. A. Lemere, Passive immunization against pyroglutamate-3 amyloid-β reduces plaque burden in Alzheimer-like transgenic mice: A pilot study. *Neurodegener. Dis.* **10**, 265–270 (2012).
22. D. L. Brody, D. M. Holtzman, Active and passive immunotherapy for neurodegenerative disorders. *Annu. Rev. Neurosci.* **31**, 175–193 (2008).
23. T. E. Golde, L. S. Schneider, E. H. Koo, Anti-aβ therapeutics in Alzheimer's disease: The need for a paradigm shift. *Neuron* **69**, 203–213 (2011).
24. S. Rasool, H. Martinez-Coria, J. W. Wu, F. LaFerla, C. G. Glabe, Systemic vaccination with anti-oligomeric monoclonal antibodies improves cognitive function by reducing Aβ deposition and tau pathology in 3xTg-AD mice. *J. Neurochem.* **126**, 473–482 (2013).
25. M. Costa, A. M. Ortiz, J. I. Jorquera, Therapeutic albumin binding to remove amyloid-β. *J. Alzheimers Dis.* **29**, 159 (2012).
26. S. J. Henderson, C. Andersson, R. Narwal, J. Janson, T. J. Goldschmidt, P. Appelkvist, A. Bogstedt, A. C. Steffen, U. Haupts, J. Tebbe, P. O. Freskgärd, L. Jermutus, M. Burrell, S. B. Fowler, C. I. Webster, Sustained peripheral depletion of amyloid-β with a novel form of neprilysin does not affect central levels of amyloid-β. *Brain* **137**, 553–564 (2014).
27. A. Alonso, E. Reinz, M. Fatar, M. G. Hennerici, S. Meairs, Clearance of albumin following ultrasound-induced blood-brain barrier opening is mediated by glial but not neuronal cells. *Brain Res.* **1411**, 9–16 (2011).
28. J. Milojevic, M. Costa, A. M. Ortiz, J. I. Jorquera, G. Melacini, In vitro amyloid-β binding and inhibition of amyloid-β self-association by therapeutic albumin. *J. Alzheimers Dis.* **38**, 753–765 (2014).
29. S. Y. Wu, Y. S. Tung, F. Marquet, M. Downs, C. Sanchez, C. Chen, V. Ferrera, E. Konofagou, Transcranial cavitation detection in primates during blood-brain barrier opening-a performance assessment study. *IEEE Trans. Ultrason. Ferroelectr. Freq. Control* **61**, 966–978 (2014).
30. K. M. Lucin, T. Wyss-Coray, Immune activation in brain aging and neurodegeneration: Too much or too little? *Neuron* **64**, 110–122 (2009).
31. M. Kinoshita, N. McDannold, F. A. Jolesz, K. Hynynen, Noninvasive localized delivery of Herceptin to the mouse brain by MRI-guided focused ultrasound-induced blood–brain barrier disruption. *Proc. Natl. Acad. Sci. U.S.A.* **103**, 11719–11723 (2006).
32. J. F. Jordão, C. A. Ayala-Grosso, K. Markham, Y. Huang, R. Chopra, J. McLaurin, K. Hynynen, I. Aubert, Antibodies targeted to the brain with image-guided focused ultrasound reduces amyloid-β plaque load in the TgCRND8 mouse model of Alzheimer's disease. *PLOS One* **5**, e10549 (2010).

33. E. Thévenot, J. F. Jordão, M. A. O'Reilly, K. Markham, Y. Q. Weng, K. D. Foust, B. K. Kaspar, K. Hynynen, I. Aubert, Targeted delivery of self-complementary adeno-associated virus serotype 9 to the brain, using magnetic resonance imaging-guided focused ultrasound. *Hum. Gene Ther.* **23**, 1144–1155 (2012).
34. J. F. Jordão, E. Thévenot, K. Markham-Coultes, T. Scarcelli, Y. Q. Weng, K. Xhima, M. O'Reilly, Y. Huang, J. McLaurin, K. Hynynen, I. Aubert, Amyloid-β plaque reduction, endogenous antibody delivery and glial activation by brain-targeted, transcranial focused ultrasound. *Exp. Neurol.* **248**, 16–29 (2013).
35. C. Sturchler-Pierrat, D. Abramowski, M. Duke, K. H. Wiederhold, C. Mistl, S. Rothacher, B. Ledermann, K. Bürki, P. Frey, P. A. Paganetti, C. Waridel, M. E. Calhoun, M. Jucker, A. Probst, M. Staufenbiel, B. Sommer, Two amyloid precursor protein transgenic mouse models with Alzheimer disease-like pathology. *Proc. Natl. Acad. Sci. U.S.A.* **94**, 13287–13292 (1997).
36. D. R. Thal, U. Rüb, M. Orantes, H. Braak, Phases of Aβ-deposition in the human brain and its relevance for the development of AD. *Neurology* **58**, 1791–1800 (2002).
37. H. W. Morrison, J. A. Filosa, A quantitative spatiotemporal analysis of microglia morphology during ischemic stroke and reperfusion. *J. Neuroinflammation* **10**, 4 (2013).

Acknowledgments: We thank M. Staufenbiel (Novartis) for the APP23 mice; T. Palliyaguru for tissue extraction and Western blot analysis; N. Cummins, S. Ellis, and H. Evans for help with data analysis; D. Blackmore and J. Vukovic for advice on behavioral tests; J. Ellis and R. Sullivan for histological tests; L. Hammond for expert confocal analysis and image processing; L. Wernbacher, T. Hitchcock, and the animal care team for animal maintenance; E. Konofagou (Columbia University) and R. Seip (Philips Research) for advice on ultrasound; and R. Tweedale for reading of the manuscript. **Funding:** This study was supported by the Estate of Dr. Clem Jones AO as well as grants from the Australian Research Council (ARC; DP130101932) and the National Health and Medical Research Council of Australia (APP1037746 and APP1003150) to J.G. Funding for microscopes was through the ARC Linkage Infrastructure, Equipment, and Facilities scheme [LE130100078]. **Author contributions:** J.G. provided funding and conceived the study, J.G. and G.L. designed the experiments, G.L. performed the experiments, and J.G. and G.L. analyzed the data and wrote the paper. **Competing interests:** A provisional patent entitled "Neurodegenerative disease treatment" has been filed. Application number: 2014902366. Filing date: 20 June 2014. **Data and materials availability:** Materials are available upon request.

Submitted 7 November 2014
Accepted 20 February 2015
Published 11 March 2015
10.1126/scitranslmed.aaa2512

Citation: G. Leinenga, J. Götz, Scanning ultrasound removes amyloid-β and restores memory in an Alzheimer's disease mouse model. *Sci. Transl. Med.* **7**, 278ra33 (2015).

Science Translational Medicine AAAS

Scanning ultrasound removes amyloid-β and restores memory in an Alzheimer's disease mouse model

Gerhard Leinenga and Jürgen Götz (March 11, 2015)
Science Translational Medicine **7** (278), 278ra33. [doi: 10.1126/scitranslmed.aaa2512]

Editor's Summary

Can ultrasound restore memory?

Transgenic mice with increased amyloid-β (Aβ) production show several aspects of Alzheimer's disease, including A β deposition and memory impairment. By repeatedly treating these Aβ-forming mice with scanning ultrasound, Leinenga and Götz now demonstrate that A β is removed and memory is restored as revealed by improvement in three memory tasks. These improvements were achieved without the use of any therapeutic agent, and the scanning ultrasound treatment did not induce any apparent damage to the mouse brain. The authors then showed that scanning ultrasound activated resident microglial cells that took up Aβ into their lysosomes. These findings suggest that repeated scanning ultrasound may be a noninvasive method with potential for treating Alzheimer's disease.

Science Translational Medicine (print ISSN 1946-6234; online ISSN 1946-6242) is published weekly, except the last week in December, by the American Association for the Advancement of Science, 1200 New York Avenue, NW, Washington, DC 20005.